Published in final edited form as:
Biochemistry. 2007 October 23; 46(42): 11753–11760. doi:10.1021/bi701177j.

Heme Attachment Motif Mobility Tunes Cytochrome *c* Redox Potential†

Lea V. Michel[‡], **Tao Ye**[§], **Sarah E. J. Bowman**[||], **Benjamin D. Levin**[||], **Megan A. Hahn**[||], **Brandy S. Russell**[||,⊥], **Sean J. Elliott**[§], and **Kara L. Bren**[*,||]
Department of Chemistry, University of Rochester, Rochester, NY 14627-0216

Abstract

Hydrogen exchange (HX) rates and midpoint potentials (E_m) of variants of cytochromes *c* from *Pseudomonas aeruginosa* (*Pa* cyt c_{551}) and *Hydrogenobacter thermophilus* (*Ht* cyt c_{552}) have been characterized toward developing an understanding of the impact of properties of the Cys-X-X-Cys-His pentapeptide *c*-heme attachment motif (CXXCH) on heme redox potential. Despite structural conservation of the CXXCH motif, *Ht* cyt c_{552} exhibits low protection from HX for amide protons within this motif relative to *Pa* cyt c_{551}. Site-directed mutants have been prepared to determine the structural basis for and functional implications of these variations in HX behavior. The double mutant *Ht*-M13V/K22M displays suppressed HX within the CXXCH motif as well as decreased E_m (by 81 mV), whereas the corresponding double mutant of *Pa* cyt c_{551} (V13M/M22K) exhibits enhanced HX within the CXXCH pentapeptide and a modest increase in E_m (by 30 mV). The changes in E_m correlate with changes in axial His chemical shifts in the ferric proteins reflecting extent of histidinate character. Thus the mobility of the CXXCH pentapeptide is found to impact the His-Fe(III) interaction and therefore heme redox potential.

Electron transfer reactions involving iron-protoporphyrin IX (heme) are central to fundamental biological processes such as respiration, redox catalysis, sensing, and signaling (1–5). A key parameter determining energetics and kinetics of electron transfer is the redox potential (1), thus, much emphasis has been placed on understanding the role of protein structure in tuning heme redox potential. Two fundamental features known to have a substantial influence on heme redox potentials are the nature of the ligands coordinated to the metal and the burial of the heme in the hydrophobic protein core. Nature alters the electron donating properties of the coordinating ligands through choice of ligands (6), modulating metal-ligand bond strength (6–12), varying coordination geometry (5), and hydrogen bonding to ligands (13–15). The encapsulation of the heme within a protein's interior also is significant for determining potential, as the hydrophobic environment favors the ferrous state over the ferric (7,8,10,16, 17). Although there have been many studies of the effects of static polypeptide structure on heme-ligand interactions and on heme burial, the role of protein mobility has received less attention. Protein motions may indeed be important as they could influence metal-ligand interactions (15,18,19) and solvent exposure.

†This work supported by National Institutes of Health Grant GM63170 (K.L.B.), a Fellowship from the Alfred P. Sloan Foundation (K.L.B.), and National Science Foundation Grant MCB-0546323 (S.J.E.).

*To whom correspondence should be addressed: Department of Chemistry, University of Rochester, Rochester, NY 14627-0216. Telephone: (585) 275-4335. Fax: (585) 276-0205. e-mail: bren@chem.rochester.edu.
‡Department of Biochemistry and Biophysics, University of Rochester, Rochester, NY 14642
§Department of Chemistry, Boston University, Boston, MA 02215
||Department of Chemistry, University of Rochester, Rochester, NY 14627-0216
⊥Current Address: Department of Chemistry, Gustavus Adolphus College, St. Peter, MN 56082

Here, we investigate the effects of structural fluctuations of the *c*-heme motif of cytochrome *c* (cyt *c*[1]) on redox potential. The *c*-type heme is characterized by its covalent attachment to the polypeptide, usually to two Cys residues in a pentapeptide Cys-X-X-Cys-His (CXXCH) motif, in which X may be any amino acid and His is a heme axial ligand (termed the proximal His; Figure 1A) (4,20). The hypothesis tested in this study is that variations of sequence within and near the *c*-heme motif impact the energetics of the motif's conformational fluctuations, which in turn impact heme-ligand interactions and thus heme redox potential. The subjects of study are the soluble mono-heme cyts *c* from *Hydrogenobacter thermophilus* (*Ht* cyt c_{552}) and *Pseudomonas aeruginosa* (*Pa* cyt c_{551}). Although these homologues display highly similar folds and structures at the CXXCH motif (residues 12–16 using *Pa* cyt c_{551} numbering; Figure 1) (21,22), energetics of conformational fluctuations involving this pentapeptide, revealed by hydrogen exchange (HX), are surprisingly disparate. In particular, protection from HX of the amide protons of CXXCH motif residues Cys15 and His16, which donate hydrogen bonds to the Cys12 carbonyl (Figure 1B), differs greatly between these proteins. Mutations are introduced to test the roles of individual amino acids in modulating CXXCH motif fluctuations and the resulting effects on redox potential. The results indicate that conformational dynamics of the CXXCH motif play a role in tuning heme potential by influencing the His-Fe interaction.

MATERIALS AND METHODS

Protein Expression and Purification

The plasmids pETPA (Amp^r) (23,24) and pSCH552 (25) (Amp^r) were used as templates for site-directed mutagenesis of *Pa* cyt c_{551} and *Ht* cyt c_{552}, respectively. Mutants (*Pa*-V13M, *Pa*-M22K, *Pa*-V13M/M22K, *Ht*-M13V, *Ht*-K22M, and *Ht*-M13V/K22M) were prepared using the QuikChange II kit (Stratagene). *Ht* cyts c_{552} and *Pa* cyts c_{551} were expressed and purified as previously described for the wild-type proteins (23,25). Preparation of uniformly ^{15}N-labeled proteins was by expression on minimal medium containing [^{15}N, 99%]NH_4Cl (Cambridge Isotope Laboratories, Inc.) as the sole nitrogen source as described (23,26).

Collection and Analysis of NOESY Data

All NMR data were collected on a Varian INOVA 500-MHz spectrometer (operating at 499.839 MHz for ^1H) at 299 K. Collection of NOESY and TOCSY spectra of oxidized *Ht*-M13V/K22M and *Pa*-V13M/M22K (3 mM in 50 mM NaP_i, pH 6.0, 5× molar excess $K_3[Fe(CN)_6]$) for analysis of heme pocket structure was as described for wild-type proteins (23, 25). Assignments were made using standard methods, assisted by assignments available in the literature (23,25,27).

Collection and Analysis of HX Data

HX was initiated by adding 500 mL D_2O to ~ 14 mg *Pa* cyt c_{551}, *Pa*-V13M, *Pa*-M22K, *Pa*-V13M/M22K, *Ht* cyt c_{552}, *Ht*-M13V, *Ht*-K22M, or *Ht*-M13V/K22M which had been lyophilized from H_2O containing 5× excess $K_3[Fe(CN)_6]$ in 50 mM NaP_i, pH 6.0. The measured pH* (uncorrected) after initiation of exchange was 6.1 for all samples. Acquisition of 2-D TOCSY or HSQC (of ^{15}N-labeled proteins) data commenced ~7 minutes after initiation of exchange. TOCSY spectra were collected (32 scans, 4096 × 256 points, 1.1-second recycle time) without solvent suppression at 8, 14, 19, 25, 30, 35, 40, 95, and 315 hours after initiation of exchange. For *Ht* cyt c_{552}, TOCSY spectra also were collected at 800, 1450, and 2650 hours after initiation of exchange. In between NMR experiments, samples were kept at 299 K in a water bath. HX experiments were performed on ^{15}N-labeled protein samples prepared as

[1]Abbreviations: cyt *c*: cytochrome *c;* E_m: electrochemical midpoint potential; *Ht* cyt c_{552}: *Hydrogenobacter thermophilus* cytochrome c_{552}; HX: hydrogen exchange; NMR: nuclear magnetic resonance; *Pa* cyt c_{551}: *Pseudomonas aeruginosa* cytochrome c_{551}; PDB: Protein Data Bank; PFV: Protein film voltammetryz

described above by collecting 3 hours of consecutive HSQC spectra (2048 × 32 points, recycle time = 1.5 seconds) at 299 K after initiation of exchange, followed by spectra at ~7 hours, ~16 hours, and ~20 hours after initiation. NMR data were processed using Felix 97 (Accelrys). Resonance assignments were determined using standard methods, assisted by published assignments (23,27,28). Peak intensities in TOCSY spectra were normalized using peaks of non-exchangeable protons as references. Cross-peak intensities at various delay times ($I(t)$) were plotted against delay time (t), and fit using KaleidaGraph (Synergy software) to a three-parameter single-exponential equation $I,(t) = A + B\exp(-k_{obs}\,t)$, to determine k_{obs}, the observed proton exchange rate. It was verified that exchange occurred in the EX2 limit (29) by observation of the expected ~10× decrease in exchange rates at pH 5.0. Protons in *Ht* cyt c_{552} that exchanged too slowly to determine an exchange rate were assigned an upper limit rate of 1.0×10^{-8} s^{-1}, which is consistent with the observation of less than 10% peak intensity change by the last time point. Protection factors (P) were calculated, according to the EX2 mechanism, as log P= log ($1/K_{op}$), where $K_{op} = k_{obs}/k_{int}$, k_{int} is the intrinsic exchange rate for the "open" form, and k_{obs} is the observed exchange rate (30,31). Values for k_{int} were determined using SPHERE (http://www.fccc.edu/research/labs/roder/sphere/) (29,31). A caveat to keep for protection factor analysis in this study is that the k_{int} values determined using SPHERE assume an unstructured polypeptide. In the case of residues at and close to the *c*-heme motif, however, the "open" form will not resemble an unstructured polypeptide. Thus, protection factors may not accurately reflect the true K_{op} value. Nevertheless, the purpose of the analysis here is to detect and interpret changes in protection factors between cyt *c* variants rather than perform a quantitative analysis of the K_{op} values themselves. This comparative analysis is valid because it is expected that perturbations of k_{int} for *c*-heme motif residues relative to an unstructured polypeptide would be similar for the different variants and species as a result of the local conservation of structure at the *c*-heme motif. Analyses of the *Ht* cyt c_{552} (22) and the *Pa* cyt c_{551} (21) crystal structures were performed using the graphics program MOLecule analysis and MOLecule display (MOLMOL) (32).

NMR Detection of Axial His Nuclei

Super-WEFT spectra (33) were collected of oxidized *Ht* cyt c_{552}, *Ht*-M13V, *Ht*-K22M, and *Ht*-M13V/K22M (1 to 3 mM protein, 50 mM NaP_i pH 7.0, 5× excess $K_3[Fe(CN)_6]$, D_2O). Side-chain protons on the Met and His axial ligands have T_1 values between 2 and 5 milliseconds, and are thus readily identified in the super-WEFT spectra. HSQC spectra of uniformly ^{15}N-labeled samples of all variants in this study (1.5 to 2 mM samples, 50 mM NaP_i, pH 7.0, 10% D_2O, 5× excess $K_3[Fe(CN)_6]$) were collected using J_{NH} values of 90 and 135 Hz. The larger J_{NH} corresponds with a shorter INEPT delay, enhancing detection of rapidly relaxing nuclei. The His16 Hδ1-Nδ cross peak was identified by its enhancement in these spectra as well as its characteristic chemical shifts, consistent with the previously reported Hδ1 shift (34).

Protein Electrochemistry

Protein film voltammetry (PFV) of cyts *c* was performed as previously described (15), with the following modifications. pH dependency studies were carried out in either a mixture of citrate and KP_i buffer (pH ranging from 2.6 to 5) or 50 mM KP_i buffer (pH 6 to 8), concentrations that ensure that phosphate ion-binding is of minimal impact to the proteins (15,35,36). Experiments conducted at scan rates higher than 500 mV/s were performed in a solution of 10 mM KP_i pH 7 buffer, in addition to 85 mM $NaNO_3$, resulting in a final ionic strength, I_{total}, of about 100 mM. Buffers were titrated with NaOH or HCl to the desired pH. The temperature of the system was maintained at 0 °C by connecting the water-jacketed electrochemical cell to a refrigerating circulator. The thermostated, electrochemical cell was housed in a Faraday cage. A polycrystalline gold wire (geometrical area = 3 mm^2), embedded in epoxy comprised the working electrode. A resin-body saturated calomel electrode (SCE,

Accumet), located in a Luggin sidearm containing 100 mM Na_2SO_4 and maintained at room temperature, was used as reference. All potentials quoted herein are against the standard hydrogen electrode. A platinum wire acted as the counter electrode to complete the three-electrode configuration. Voltammetry was conducted with an Autolab electrochemical analyzer (PG-STAT 12, Eco. Chemie, Utrecht, The Netherlands), equipped with ECD and ADC modules, and controlled by GPES software (Eco Chemie). Compensating for the IR drop within the cell was further achieved by using the IR positive feedback module of the PG-STAT 12 instrument, as needed. Electroactive protein films were generated as previously described (15), and all experiments were repeated at least three times. The data collected was subjected to analysis by subtracting a polynomial baseline to remove the non-faradaic current. The interfacial electron transfer rate constant, k^0, was determined by trumpet plot analysis (peak position of the cathodic and anodic electrochemical signals, as a function of scan rate), as described by Armstrong and co-workers (37,38).

RESULTS

Hydrogen Exchange of Wild-type Proteins

HX experiments probe energetics of conformational openings that lead to exchange of amide protons that are sequestered from solvent in the "closed" (folded) form. In what is termed the EX2 limit, the observed HX rates (k_{obs}) can be translated into protection factors (log P = log (k_{int}/k_{obs})), where k_{int} is the intrinsic exchange rate for the "open" form (30,31). Protection factors in turn are related to the free energy of the conformational opening leading to exchange ($\Delta G_{op} = RT \ln P$) (29). *Ht* cyt c_{552} and *Pa* cyt c_{551} exhibit similar overall trends in protection factors, as expected from their highly homologous secondary and tertiary structures (Supporting Figure S1). The enhanced stability of *Ht* cyt c_{552} is reflected in its generally higher protection of core residues relative to *Pa* cyt c_{551} (39,40). Proteins from thermophilic organisms, such as *Ht* cyt c_{552}, typically experience higher energy unfolding events (both global and subglobal) that lead to HX, and thus higher protection factors, as compared to mesophilic counterparts (41). For CXXCH motif residues, however, this trend is not followed, as *Pa* cyt c_{551} exhibits greater protection of Cys15 (> 10-fold) and His16 (> 100-fold; Table 1), two residues forming key hydrogen bonds within this motif to Cys12 (Figure 1; residues are CMACH in *Ht* cyt c_{552} and CVACH in *Pa* cyt c_{551}). HX analysis thus reveals that conformational excursions leading to exchange of Cys15 and His16 amide protons occur with lower energy in *Ht* cyt c_{552} compared to *Pa* cyt c_{551}.

Hydrogen Exchange of Proximal Heme Pocket Mutants

The structures of the CXXCH pentapeptide backbone in *Pa* cyt c_{551} (21) and *Ht* cyt c_{552} (22) are nearly identical (see next section). However, substantial differences in protection of CXXCH backbone amide protons from HX are seen, suggesting that variations in proximal heme pocket residues influence energetics of CXXCH motif conformational openings leading to HX. Examination of the protein structures (21,22) (Figure 2) reveals that Met13 and Asp17 in *Ht* cyt c_{552} do not pack as well as do Val13 and Ala17 in *Pa* cyt c_{551}, which may destabilize the key Cys15 and His16 interactions with Cys12 in *Ht* cyt c_{552} and result in more efficient exchange of the *Ht* cyt c_{552} His16 and Cys15 amide protons with solvent. Another notable difference is amino acid 22. In *Pa* cyt c_{551}, the hydrophobic Met22 lies across the CXXCH loop, which is expected to stabilize the loop against conformational openings. In *Ht* cyt c_{552}, residue 22 is Lys, and as a charged residue may interact with solvent more than the loop region.

To test the hypothesized roles of residues 13 and 22 in influencing local conformational fluctuations, the mutants *Ht*-M13V, *Ht*-K22M, *Pa*-V13M, *Pa*-M22K, *Ht-M*13V/K22M, and *Pa*-V13M/M22K were prepared and HX rates were determined. Focusing on the double mutants which show the largest effects, overall backbone protection is similar between the

mutants and their respective wild-type proteins (Figure S1). In the proximal pocket, however, significant decreases in protection of Cys15 and His16 in *Pa*-V13M/M22K are seen relative to wild-type, and increases for these same residues are observed for *Ht*-M13V/K22M relative to wild-type (Table 1). Particularly dramatic is the increase in protection of His16 in *Ht*-M13V/K22M by more than three orders of magnitude relative to wild-type (Figure 3). These results indicate that residues 13 and 22, particularly in combination, play key roles in controlling the energetics of opening of the CXXCH motif in these proteins. Notably, the single mutants show intermediate changes in protection, in particular for *Ht* cyt c_{552} and its variants which show the more straightforward behavior relative to *Pa* cyt c_{552} (Table 1). Interestingly, protection of Asp17 HN, which hydrogen bonds to a buried water, shows little difference between the two cyt *c* species and among the mutants, suggesting that the differences seen here between proteins are specific to the CXXCH motif itself.

Analysis of c-Heme Motif Structures

To analyze the extent to which variations in the CXXCH sequence influence local backbone structure, ten cyts *c* having disparate properties of "XX" residues in the motif and for which high-resolution (< 2.5 Å) x-ray crystal structures are available were selected for analysis (supporting Table S1). Despite differences of the variable "XX" residues, the CXXCH backbone structure is highly conserved, as it is defined primarily by the constraints of the covalent and coordinate bonds between the Cys and His residues with the heme (42, 43). In the selected group of cyts *c*, this motif displays an RMSD of 0.34 Å (for backbone atoms); *Ht* cyt c_{552} and *Pa* cyt c_{551} have an RMSD of 0.21 Å in this region (Figure 1C). Subtle structural differences are seen among the cyts *c*, as illustrated by the modest range of distances between the backbone carbonyl oxygen of the first Cys in the motif (Cys12 in *Pa* cyt c_{551}) and its hydrogen bond donors Cys15 and His16 (Table S1). Nevertheless, despite wide sequence variations, the pentapeptide backbone structure is structurally conserved across diverse sequences.

To verify that the mutations introduced here do not significantly perturb CXXCH backbone structure, NOESY spectra for wild-type and double mutant proteins were compared, and the expected pattern of NOEs within the CXXCH motif between the wild-type and double mutant proteins is observed. (Results for *Ht*-M13V/K22M and wild-type are in Supporting Table S2. A similar comparison of *Pa* cyt c_{551} and mutants was attempted but extensive chemical shift degeneracy between residues 13, 14, and 15 precluded a rigorous analysis). The overall maintenance of the NOE pattern along with the strong conservation of the motif structure across diverse cyt *c* sequences and folds indicate that significant backbone structure rearrangement upon mutation is unlikely.

Assignment and Analysis of Proximal His NMR Resonances

Chemical shifts of heme axial His ring nuclei in paramagnetic heme proteins report on the His-Fe(III) interaction. The axial His16 Hδ1-Nδ1 HSQC peak for each protein is easily identified, as it is shifted outside of the diamagnetic envelope and exhibits an increase in intensity with increased J_{NH} values used in the HSQC experiment, which enhances detection of nuclei with short relaxation times as a result of proximity to the paramagnetic iron. The Hε1 His proton resonance was identified for *Ht* cyt c_{552} and *Ht*-M13V/K22M using the 1-D super-WEFT experiment based on its very short T_1 and large upfield shift (33). Assignments for selected axial His nuclei are given in Table 2, and a plot of His16 Hδ1 chemical shift vs. E_m is shown in Figure 4. The Hε1 shift shows an increase in magnitude as E_m is lowered, reflecting increased histidinate character with lower E_m (44–49). Likewise, the His16 Hδ1 shifts upfield as E_m is lowered, consistent with enhanced hydrogen bonding as has been demonstrated previously in other low-spin ferric heme proteins (46,47).

Protein Electrochemistry

The ability to modulate energetics of conformational openings leading to HX of the CXXCH motif in *Ht* cyt c_{552} and *Pa* cyt c_{551} by selected mutations provides the opportunity to test the effects of fluctuations to which HX is sensitive on heme redox potential. Thus, the mutants were examined by protein film voltammetry (PFV) to determine electrochemical midpoint potential (E_m) as well as the interfacial electron transfer kinetics. Table 3 summarizes the observed values of E_m at pH 7. Notably, the *Ht* cyt c_{552} mutants (single and double) display lower potentials: each of the mutations resulted in a systematic shift to lower potential that is nearly additive ($E_{WT} - E_{M13V/K22M}$, 81 mV ≈ ($E_{WT} - E_{M13V}$), 59 mV + ($E_{WT} - E_{K22M}$), 37 mV). To ensure this is not merely an effect of variable pH-dependent phenomena between the mutants, the impact of pH upon E_m for the *Ht* cyts c_{552} was assessed (Figure 5). Clearly, all of the *Ht* cyts c_{552} (wild-type and mutants) display potentials that are pH independent close to neutral. Further, the same simple model of protonation holds for each of the mutants considered here, where a single pK_{red} is observed for the reduced form of the various cyts *c*, spanning a modest range of values from 4.2 to 4.7, and indicating that the mutations do not significantly alter the protonation associated with heme redox chemistry.

The *Pa* cyts c_{551} also were investigated by PFV, and the midpoint potentials at pH 7 are given in Table 3. Compared to the *Ht* cyt c_{552} mutants, a reversed trend is observed; however, the increases are smaller, and not additive as seen for the *Ht* cyt c_{552} mutants. This discrepancy may be due to differences in pH-dependent behavior, as it has been previously shown that the redox-behavior of *Pa* cyt c_{551} mutants display disrupted H^+:e^- coupling and pH dependencies of E_m that cannot be fit to previously described models of proton-binding to heme-propionate 7 (15,50). Thus, a quantitative evaluation of the exact change in potential is challenging, although the qualitative trends are clear.

In parallel experiments, interfacial electron transfer rates for each of the cyts *c* were determined by trumpet plot analysis (Supporting Figure S2). All of the proteins display fast electron transfer, with k^0 on the order of 10^3 s^{-1}, which are similar to reported k^0 values for eukaryotic cyts *c* investigated on gold electrodes (51–53).

DISCUSSION

Electrochemical Response of Mutants

We have examined the relationship between cyt *c* mutations that impact the conformational openings of the CXXCH motif, and the redox properties of the resulting mutants. Relative to wild-type, the mutants of *Ht* cyt c_{552} that have suppressed HX show a systematic decrease in E_m, whereas those of *Pa* cyt c_{551} with enhanced HX display an increase in E_m. Before linking these changes in *E*m to specific features of heme pocket mobility, we can consider several traits of the *Pa* cyt c_{551} and *Ht* cyt c_{552} mutants: electrostatic charge perturbations, alterations in the protein fold, proximal histidinate character, as well as heme conformation. For example, a possible explanation is the observed changes in E_m could arise from electrostatic perturbations caused by the mutations. Specifically, the electrostatic potential at the heme iron can be influenced by the charges of surrounding residues (54,55). Here, for example, in *Ht*-M13V/K22M, the charged Lys side-chain is replaced by a neutral side-chain, Met. However, the charge-neutral single mutation, M13V, exhibits a greater impact on redox potential than the K22M mutation (Table 3), thus suggesting that the change in charge of residue 22 is not the major contributor to the significant decrease in redox potential exhibited by *Ht*-M13V/K22M. It also is notable that the cyts *c* studied demonstrate reversible direct electrochemistry upon modified gold electrodes, indicative of rapid electron transfer kinetics (10^3 s^{-1}). Furthermore, the *Ht* cyt c_{552} mutants all behave similar to wild-type in terms of the previously characterized relationships between E_m and both phosphate ion- and proton-binding schemes (15). These

general observations suggest that the observed changes in E_m result from fundamental differences in the heme pocket and not alterations in apparent electrokinetics, pH-induced effects, or electrostatics.

Structure of Mutants

The changes in E_m for the mutants could be a result of alterations to the protein fold. The pattern of protection factors (with the exception of the proximal heme pocket residues) for the mutants is similar overall to that for the wild-type proteins; this finding argues against a global structure perturbation caused by mutation because protection from HX reflects hydrogen bonding and secondary structure (56) (Figure S2). Within the proximal heme pockets, similarity of NOE patterns for the wild-type and mutant proteins argues against major local backbone structure changes (Table S2). Indeed, no major change in structure of the CXXCH motif upon mutation is expected as this structure is highly conserved among cyts *c* despite wide variations in the identity of the "XX" and other heme pocket residues (Figure 1C;Table S1). In addition, the close similarity between the CXXCH structure in *c*-heme peptide fragments (microperoxidases) and in folded cyt *c* indicates that local coordinate and covalent bonding defines the motif's three-dimensional backbone structure (42,43). Barring changes in local polypeptide folding causing the observed changes in E_m, we propose a model in which perturbations of the redox potential can be caused by alterations of CXXCH motif mobility impacting donor properties of the proximal His. Analysis of proximal His chemical shifts support this hypothesis, as shown below. A second possible explanation discussed below is that mutations impact E_m by exerting a systematic change in heme conformation.

Effect of Mutations on Proximal His

The proximal His16 in *Ht* cyt c_{552} and *Pa* cyt c_{551} donates a hydrogen bond to the backbone carbonyl of Pro25, with an oxygen-nitrogen distance of ~2.8 Å (Figure 1A) (21, 22). Hydrogen bonding involving the axial His in heme proteins has been shown to affect the ligand's electron-donating properties, which in turn tunes redox potential (13, 14, 44, 46, 47, 57). Specifically, the stronger the hydrogen bond between the His ligand Hδ1 and the hydrogen bond acceptor, the greater the histidinate character. A more appreciable histidinate character results in the His being a better electron donor to the iron, which stabilizes the ferric oxidation state more than the ferrous and hence provides for a decrease in the redox potential. This effect has been analyzed previously by comparing the cyanide-inhibited forms of different heme proteins with different E_m values (44, 46), or by mutating residues that hydrogen bond with a proximal His residue (45). Here, we examine a more indirect effect of local CXXCH motif structure on the proximal His in cyts *c*.

Evaluation of histidinate character of the proximal His, and hydrogen bonding with the proximal His has been performed by analysis of its chemical shifts in the ferric state. The heme axial His Hδ1, the hydrogen bond donor, has been shown to display an upfield shift in the low-spin ferric proteins as E_m is lowered, other factors remaining constant (46,47). A similar correlation is seen here for the lower-potential variants of *Ht* cyt c_{552} which exhibit a systematic upfield shift of the His16 Hδ1 (as well as Nδ) resonance compared to wild-type (Figure 4;Table 2,3). In a complementary fashion, the *Pa* cyt c_{551} mutants exhibit a downfield shift of His16 Hδ1 (and Nδ) relative to wild-type. Notably, the magnitude of the change in shift correlates well with the magnitude of change in E_m, as illustrated by the similar slopes of the lines in Figure 4 (0.022 ± 0.003 and 0.025 ± 0.003 ppm/mV for *Pa* cyt c_{551} variants and for *Ht* cyt c_{552} variants, respectively). The need to consider the shifts of each protein species separately is a result of differences in the pseudocontact contribution to chemical shift, as the two proteins have different heme axial Met orientations and thus different magnetic anisotropies and orientations of magnetic axes (28). Because of the large error in calculating the significant pseudocontact contribution to chemical shift for the His ligand, correction for this difference

has not been made. The magnitude of the axial His Hε1 chemical shifts also has been related to extent of histidinate character (44–49). In step with other results here, the *Ht* cyt c_{552} mutants generally display an upfield shift of His16 Hε1 relative to wild-type (Table 2). The His16 Hε1 of *Pa* cyt c_{551} could not be assigned.

We next consider how variations in CXXCH motif mobility reflected by HX may cause the observed differences in hydrogen bonding to the proximal His and the His-Fe(III) interaction. Changes in HX protection of the Cys15 and His16 amide protons directly report on conformational openings of the CXXCH motif as they form key hydrogen bonds with Cys12 carbonyl (Figure 1B). Thus, the greater protection of these residues in *Ht*-M13V/K22M relative to wild-type (Table 1) reflects a more rigid CXXCH structure with suppressed conformational excursions to an open form. Decreased CXXCH mobility in turn is correlated here with lower E_m. A basis for the observed correlation is that higher CXXCH mobility interferes mechanically with the maintenance of the His16 Hδ1-Pro25 CO hydrogen bond, reducing histidinate character and increasing E_m for variants with enhanced HX. An alternative related explanation for the lower E_m in variants with suppressed HX is that lower (transient) access of water to the proximal heme pocket enhances hydrogen bonding between His16 and Pro25 by excluding competing hydrogen bonding groups (water) and/or by decreasing local dielectric.

A comparison of HX behavior of mitochondrial ferric cyt b_5 (OM b_5) to microsomal ferric cyt b_5 (Mc b_5) has previously invoked a role of heme pocket mobility in tuning redox potential (18). HX results reveal that OM b_5 undergoes higher energy unfolding events in the heme pocket compared to Mc b_5, indicating less conformational mobility surrounding one of the His axial ligands in the former protein. The resulting tighter hydrophobic packing around the heme active site is proposed to yield stronger His-Fe(III) coordination in OM b_5, which may account for its lower redox potential (18). A similar effect has been invoked in a study of model heme-peptide compounds, in which high peptide mobility has been correlated with high redox potential. The high heme potential is proposed to result from preferential weakening of the His-Fe(III) bond relative to the His-Fe(II) bond (19).

Possible Role of Heme Conformation

Studies of *c*-heme peptides (microperoxidases) have shown that the CXXCH motif is sufficient to induce the significant distortion of heme from planarity toward the ruffled conformation that is typically seen in *c*-type cytochromes (58,59). In addition, an enhanced hydrophobic environment for this motif (provided by encapsulation of microperoxidase in a reverse micelle in model studies), is proposed to augment the buckling force of the CXXCH pentapeptide on the heme by strengthening the characteristic backbone hydrogen bonds within the CXXCH motif (58,60). The changes in protection for the variants here may reflect a similar effect; the variants with suppressed HX have enhanced hydrogen bonding within the CXXCH motif, which may increase heme distortion. The increased distortion, in turn, would decrease redox potential (59,61), consistent with our observations.

Summary

The extent of protection of the residues within the CXXCH region is highly variable among cyt *c* species, despite the conservation of local backbone structure. In particular, great variability is observed in the protection of the backbone amide protons of the His axial ligand and the preceding Cys residue, defining the key intra-motif hydrogen bonding interactions with the first Cys carbonyl (Figure 1B). (For examples of differences in protection among oxidized cyts *c*, see references (23, 62–64). Note that such comparisons must be made with caution as data were collected under a range of conditions). The different propensities for conformational opening of the CXXCH motif, modulated by identity of the variable residues within and near

the signature pentapeptide, indeed may play a role in tuning heme redox potential by influencing His donor properties and/or heme conformation. Further studies of this possible relationship will be probed in the future by addressing the relative enthalpic and entropic contributions to E_m for the individual mutants. We conclude that variations in heme pocket mobility should be considered when accounting for factors impacting E_m (18, 19) in addition to the "static" factors traditionally invoked.

Supplementary Material

Refer to Web version on PubMed Central for supplementary material.

Acknowledgements

We are grateful to Linda Thöny-Meyer for the gift of pEC86, and Francesca Cutruzzolà for the gift of pETPA.

References

1. Marcus RA, Sutin N. Electron transfers in chemistry and biology. Biochim Biophys Acta 1985;811:265–322.
2. Gray HB, Winkler JR. Electron tunneling through proteins. Q Rev Biophys 2003;36:341–372. [PubMed: 15029828]
3. Paoli M, Marles-Wright J, Smith A. Structure-function relationships in heme-proteins. DNA Cell Biol 2002;21:271–280. [PubMed: 12042067]
4. Bertini I, Cavallaro G, Rosato A. Cytochrome *c*: Occurrence and functions. Chem Rev 2006;106:90–115. [PubMed: 16402772]
5. Walker FA. Models of the bis-histidine-ligated electron-transferring cytochromes. Comparative geometric and electronic structure of low-spin ferro- and ferrihemes. Chem Rev 2004;104:589–615. [PubMed: 14871136]
6. Raphael AL, Gray HB. Semisynthesis of axial ligand (position-80) mutants of cytochrome *c*. J Am Chem Soc 1991;113:1038–1040.
7. Tezcan FA, Winkler JR, Gray HB. Effects of ligation and folding on reduction potentials of heme proteins. J Am Chem Soc 1998;120:13383–13388.
8. Mao JJ, Hauser K, Gunner MR. How cytochromes with different folds control heme redox potentials. Biochemistry 2003;42:9829–9840. [PubMed: 12924932]
9. Kennedy ML, Silchenko S, Houndonougbo N, Gibney BR, Dutton PL, Rodgers KR, Benson DR. Model hemoprotein reduction potentials: The effects of histidine-to-iron coordination equilibrium. J Am Chem Soc 2001;123:4635–4636. [PubMed: 11457264]
10. Battistuzzi G, Bellei M, Borsari M, Di Rocco G, Ranieri A, Sola M. Axial ligation and polypeptide matrix effects on the reduction potential of heme proteins probed on their cyanide adducts. J Biol Inorg Chem 2005;10:643–651. [PubMed: 16133205]
11. Cowley AB, Lukat-Rodgers GS, Rodgers KR, Benson DR. A possible role for the covalent heme-protein linkage in cytochrome *c* revealed via comparison of N-acetylmicroperoxidase-8 and a synthetic, monohistidine-coordinated heme peptide. Biochemistry 2004;43:1656–1666. [PubMed: 14769043]
12. Reedy CJ, Gibney BR. Heme protein assemblies. Chem Rev 2004;104:617–649. [PubMed: 14871137]
13. O'Brien P, Sweigart DA. Effect on redox potentials of hydrogen bonding from coordinated imidazole in metalloporphyrin complexes. Inorg Chem 1985;24:1405–1409.
14. Quinn R, Mercer-Smith J, Burstyn JN, Valentine JS. Influence of hydrogen bonding on the properties of iron porphyrin imidazole complexes - An internally hydrogen-bonded imidazole ligand. J Am Chem Soc 1984;106:4136–4144.
15. Ye T, Kaur R, Wen X, Bren KL, Elliott SJ. Redox properties of wild-type and heme-binding loop mutants of bacterial cytochromes *c* measured by direct electrochemistry. Inorg Chem 2005;44:8999–9006. [PubMed: 16296855]

16. Churg AK, Warshel A. Control of the redox potential of cytochrome *c* and microscopic dielectric effects in proteins. Biochemistry 1986;25:1675–1681. [PubMed: 3011070]

17. Shifman JM, Gibney BR, Sharp RE, Dutton PL. Heme redox potential control in de novo designed four-alpha-helix bundle proteins. Biochemistry 2000;39:14813–14821. [PubMed: 11101297]

18. Simeonov M, Altuve A, Massiah MA, Wang A, Eastman MA, Benson DR, Rivera M. Mitochondrial and microsomal ferric *b*-5 cytochromes exhibit divergent conformational plasticity in the context of a common fold. Biochemistry 2005;44:9308–9319. [PubMed: 15981997]

19. Cowley AB, Kennedy ML, Silchenko S, Lukat-Rodgers GS, Rodgers KR, Benson DR. Insight into heme protein redox potential control and functional aspects of six-coordinate ligand-sensing heme proteins from studies of synthetic heme peptides. Inorg Chem 2006;45:9985–10001. [PubMed: 17140194]

20. Scott, RA.; Mauk, AG. Cytochrome c: A Multidisciplinary Approach. University Science Books; Sausalito, CA: 1996.

21. Matsuura Y, Takano T, Dickerson RE. Structure of cytochrome *c*-551 from *Pseudomonas aeruginosa* refined at 1.6-Å resolution and comparison of the 2 redox forms. J Mol Biol 1982;156:389–409. [PubMed: 6283101]

22. Travaglini-Allocatelli C, Gianni S, Dubey VK, Borgia A, Di Matteo A, Bonivento D, Cutruzzolà F, Bren KL, Brunori M. An obligatory intermediate in the folding pathway of cytochrome *c*-552 from *Hydrogenobacter thermophilus*. J Biol Chem 2005;280:25729–25734. [PubMed: 15883159]

23. Russell BS, Zhong L, Bigotti MG, Cutruzzolà F, Bren KL. Backbone dynamics and hydrogen exchange of *Pseudomonas aeruginosa* ferricytochrome *c*-551. J Biol Inorg Chem 2003;8:156–166. [PubMed: 12459911]

24. Wen X, Bren KL. Heme axial methionine fluxion in *Pseudomonas aeruginosa* Asn64Gln cytochrome *c*-551. Inorg Chem 2005;44:8587–8593. [PubMed: 16271000]

25. Karan EF, Russell BS, Bren KL. Characterization of *Hydrogenobacter thermophilus* cytochromes *c*-552 expressed in the cytoplasm and periplasm of *Escherichia coli*. J Biol Inorg Chem 2002;7:260–272. [PubMed: 11935350]

26. Morar AS, Kakouras D, Young GB, Boyd J, Pielak GJ. Expression of N-15-labeled eukaryotic cytochrome *c* in *Escherichia coli*. J Biol Inorg Chem 1999;4:220–222. [PubMed: 10499094]

27. Timkovich R, Cai ML. Investigation of the structure of oxidized *Pseudomonas aeruginosa* cytochrome *c*-551 by NMR - Comparison of observed paramagnetic shifts and calculated pseudocontact shifts. Biochemistry 1993;32:11516–11523. [PubMed: 8218218]

28. Zhong L, Wen X, Rabinowitz TM, Russell BS, Karan EF, Bren KL. Heme axial methionine fluxionality in *Hydrogenobacter thermophilus* cytochrome *c*-552. Proc Natl Acad Sci USA 2004;101:8637–8642. [PubMed: 15161973]

29. Englander SW, Kallenbach NR. Hydrogen exchange and structural dynamics of proteins and nucleic acids. Q Rev Biophys 1983;16:521–655. [PubMed: 6204354]

30. Hvidt A, Nielsen SO. Hydrogen exchange in proteins. Adv Prot Chem 1966;21:287–386.

31. Bai YW, Milne JS, Mayne L, Englander SW. Primary structure effects on peptide group hydrogen exchange. Proteins 1993;17:75–86. [PubMed: 8234246]

32. Koradi R, Billeter M, Wüthrich K. MOLMOL: A program for display and analysis of macromolecular structures. J Mol Graph 1996;14:51. [PubMed: 8744573]

33. Inubushi T, Becker ED. Efficient detection of paramagnetically shifted NMR resonances by optimizing the WEFT pulse sequence. J Mag Res 1983;51:128–133.

34. Tachiiri N, Hemmi H, Takayama SJ, Mita H, Hasegawa J, Sambongi Y, Yamamoto Y. Effects of axial methionine coordination on the in-plane asymmetry of the heme electronic structure of cytochrome *c*. J Biol Inorg Chem 2004;9:733–742. [PubMed: 15235942]

35. Brautigan DL, Ferguson-Miller SG, Margoliash E. Definition of cytochrome *c* binding domains by chemical modification. I Reaction with 4-chloro-3,5-dinitrobenzoate and chromatographic separation of singly substituted derivatives. J Biol Chem 1978;253:130–139. [PubMed: 201614]

36. Margalit R, Schejter A. Cytochrome *c* - Thermodynamic study of relationships among oxidation state, ion-binding, and structural parameters. 1 Effects of temperature, pH and electrostatic media on standard redox potential of cytochrome *c*. Eur J Biochem 1973;32:492–499. [PubMed: 4348126]

37. Armstrong FA, Camba R, Heering HA, Hirst J, Jeuken LJC, Jones AK, Léger C, McEvoy JP. Fast voltammetric studies of the kinetics and energetics of coupled electron-transfer reactions in proteins. Faraday Discuss 2000:191–203. [PubMed: 11197478]
38. Hirst J, Armstrong FA. Fast-scan cyclic voltammetry of protein films on pyrolytic graphite edge electrodes: Characteristics of electron exchange. Anal Chem 1998;70:5062–5071. [PubMed: 9852788]
39. Uchiyama S, Ohshima A, Nakamura S, Hasegawa J, Terui N, Takayama SIJ, Yamamoto Y, Sambongi Y, Kobayashi Y. Complete thermal unfolding profiles of oxidized and reduced cytochromes *c*. J Am Chem Soc 2004;126:14684–14685. [PubMed: 15535669]
40. Wen X, Patel KM, Russell BS, Bren KL. Effects of heme pocket structure and mobility on cytochrome *c* stability. Biochemistry 2007;46:2537–2544. [PubMed: 17279778]
41. Závodszky P, Kardos J, Svingor Á, Petsko GA. Adjustment of conformational flexibility is a key event in the thermal adaptation of proteins. Proc Natl Acad Sci USA 1998;95:855–871.
42. Low DW, Gray HB, Duus JØ. Paramagnetic NMR spectroscopy of microperoxidase-8. J Am Chem Soc 1997;119:1–5.
43. Ma JG, Laberge M, Song XZ, Jentzen W, Jia SL, Zhang J, Vanderkooi JM, Shelnutt JA. Protein-induced changes in nonplanarity of the porphyrin in nickel cytochrome *c* probed by resonance Raman spectroscopy. Biochemistry 1998;37:5118–5128. [PubMed: 9548742]
44. La Mar GN, de Ropp JS, Chacko VP, Satterlee JD, Erman JE. Axial histidyl imidazole non-exchangeable proton resonances as indicators of imidazole hydrogen-bonding in ferric cyanide complexes of heme peroxidases. Biochim Biophys Acta 1982;708:317–325. [PubMed: 6293582]
45. Satterlee JD, Erman JE, Mauro JM, Kraut J. Comparative proton NMR analysis of wild-type cytochrome *c* peroxidase from yeast, the recombinant enzyme from *Escherichia coli*, and an Asp235Asn mutant. Biochemistry 1990;29:8797–8804. [PubMed: 2176836]
46. Banci L, Bertini I, Turano P, Tien M, Kirk TK. Proton NMR investigation into the basis for the relatively high redox potential of lignin peroxidase. Proc Natl Acad Sci USA 1991;88:6956–6960. [PubMed: 11607206]
47. Banci L, Bertini I, Kuan IC, Tien M, Turano P, Vila AJ. NMR investigation of isotopically labeled cyanide derivatives of lignin peroxidase and manganese peroxidase. Biochemistry 1993;32:13483–13489. [PubMed: 8257683]
48. Ferrer JC, Turano P, Banci L, Bertini I, Morris IK, Smith KM, Smith M, Mauk AG. Active-site coordination chemistry of the cytochrome *c* peroxidase Asp235Ala variant - Spectroscopic and functional characterization. Biochemistry 1994;33:7819–7829. [PubMed: 8011646]
49. de Ropp JS, Sham S, Asokan A, Newmyer S, de Montellano PRO, La Mar GN. Influence of the distal His in imparting imidazolate character to the proximal His in heme peroxidase: H-1 NMR spectroscopic study of cyanide-inhibited His42 -> Ala horseradish peroxidase. J Am Chem Soc 2002;124:11029–11037. [PubMed: 12224950]
50. Leitch FA, Moore GR, Pettigrew GW. Structural basis for the variation of pH-Dependent redox potentials of *Pseudomonas* cytochromes *c*-551. Biochemistry 1984;23:1831–1838. [PubMed: 6326813]
51. Song S, Clark RA, Bowden EF, Tarlov MJ. Characterization of cytochrome *c* alkanethiolate structures prepared by self-assembly on gold. J Phys Chem 1993;97:6564–6572.
52. Avila A, Gregory BW, Niki K, Cotton TM. An electrochemical approach to investigate gated electron transfer using a physiological model system: Cytochrome *c* immobilized on carboxylic acid-terminated alkanethiol self-assembled monolayers on gold electrodes. J Phys Chem B 2000;104:2759–2766.
53. Niki K, Hardy WR, Hill MG, Li H, Sprinkle JR, Margoliash E, Fujita K, Tanimura R, Nakamura N, Ohno H, Richards JH, Gray HB. Coupling to lysine-13 promotes electron tunneling through carboxylate-terminated alkanethiol self-assembled monolayers to cytochrome *c*. J Phys Chem B 2003;107:9947–9949.
54. Gunner MR, Honig B. Electrostatic control of midpoint potentials in the cytochrome subunit of the *Rhodopseudomonas viridis* reaction center. Proc Natl Acad Sci USA 1991;88:9151–9155. [PubMed: 1924378]

55. Voigt P, Knapp EW. Tuning heme redox potentials in the cytochrome *c* subunit of photosynthetic reaction centers. J Biol Chem 2003;278:51993–52001. [PubMed: 12975370]
56. Milne JS, Mayne L, Roder H, Wand AJ, Englander SW. Determinants of protein hydrogen exchange studied in equine cytochrome *c*. Protein Sci 1998;7:739–745. [PubMed: 9541406]
57. Goodin DB, McRee DE. The Asp-His-Fe triad of cytochrome *c* peroxidase controls the reduction potential, electronic structure, and coupling of the tryptophan free radical to the heme. Biochemistry 1993;32:3313–3324. [PubMed: 8384877]
58. Ma JG, Vanderkooi JM, Zhang J, Jia SL, Shelnutt JA. Resonance Raman investigation of nickel microperoxidase-11. Biochemistry 1999;38:2787–2795. [PubMed: 10052950]
59. Jentzen W, Ma JG, Shelnutt JA. Conservation of the conformation of the porphyrin macrocycle in hemoproteins. Biophys J 1998;74:753–763. [PubMed: 9533688]
60. Ma JG, Zhang J, Franco R, Jia SL, Moura I, Moura JJG, Kroneck PMH, Shelnutt JA. The structural origin of nonplanar heme distortions in tetraheme ferricytochromes *c*-3. Biochemistry 1998;37:12431–12442. [PubMed: 9730815]
61. Barkigia KM, Chantranupong L, Smith KM, Fajer J. Structural and theoretical models of photosynthetic chromophores - Implications for redox, light-absorption properties and vectorial electron flow. J Am Chem Soc 1988;110:7566–7567.
62. Bartalesi I, Rosato A, Zhang W. Hydrogen exchange in a bacterial cytochrome *c*: A fingerprint of the cytochrome *c* fold. Biochemistry 2003;42:10923–10930. [PubMed: 12974626]
63. Marmorino JL, Auld DS, Betz SF, Doyle DF, Young GB, Pielak GJ. Amide proton exchange rates of oxidized and reduced *Saccharomyces cerevisiae* iso-1-cytochrome *c*. Protein Sci 1993;2:1966–1974. [PubMed: 8268806]
64. Bai YW, Sosnick TR, Mayne L, Englander SW. Protein folding intermediates - Native state hydrogen exchange. Science 1995;269:192–197. [PubMed: 7618079]
65. Kraulis PJ. Molscript - A program to produce both detailed and schematic plots of protein structures. J Appl Crystallogr 1991;24:946–950.
66. Humphrey W, Dalke A, Schulten K. VMD: Visual molecular dynamics. J Mol Graph 1996;14:33. [PubMed: 8744570]

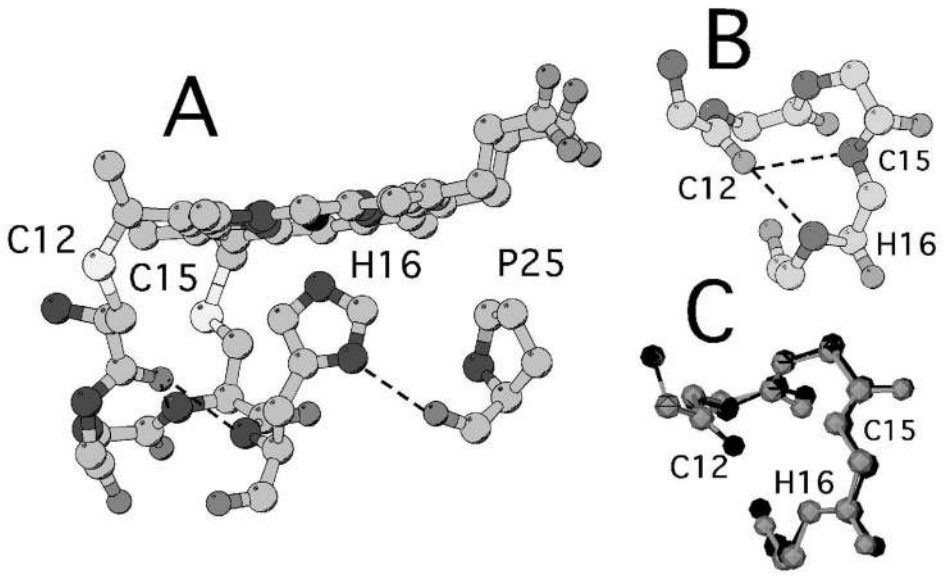

Figure 1.

(A) Heme and CXXCH motif (residues 12–16) and Pro25 from *Pa* cyt c_{551} (PDB: 351C) (21). The side chains of residues 13, 14, and 15 are omitted for clarity. The hydrogen bond between Pro25 carbonyl and the proximal His16 Hδ1 is indicated with a dashed line. Figure prepared using Molscript (65). (B) Structure of CXXCH motif from *Pa* cyt c_{551}. The intra-motif hydrogen bonds between the Cys12 carbonyl and the backbone HN groups of Cys15 and His16 are indicated with dashed lines. In (A) and (B), nitrogen atoms are dark gray, oxygen medium gray, and sulfur the lightest shade. (C) Overlay (RMSD 0.21 Å) of backbone of CXXCH motif from *Pa* cyt c_{551} (silver) and *Ht* cyt c_{552} (black) (PDB: 1YNR) (22). Figure prepared using VMD (66).

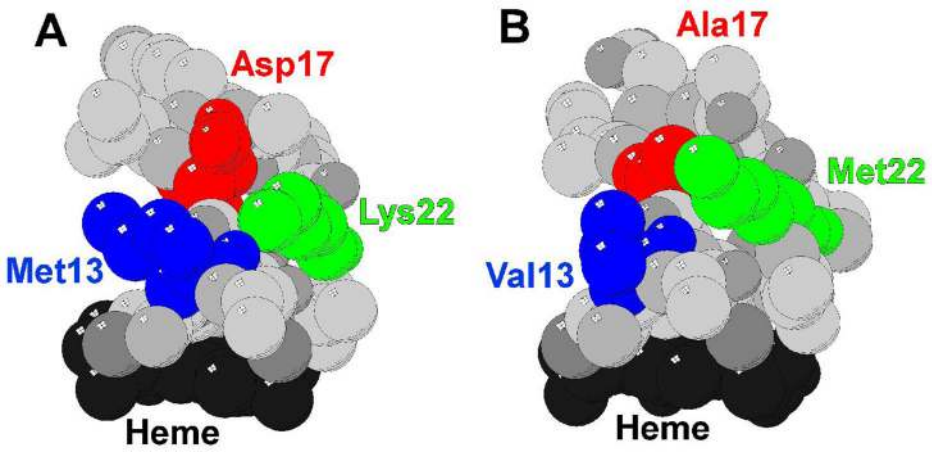

Figure 2.

Space-filling representation of proximal heme pocket of (A) *Ht* cyt c_{552} (PDB: 1YNR) (22) and (B) *Pa* cyt c_{551} (PDB: 351C) (21) highlighting residues targeted for mutation (13 (blue) and 22 (green)) as well as residue 17 (red).

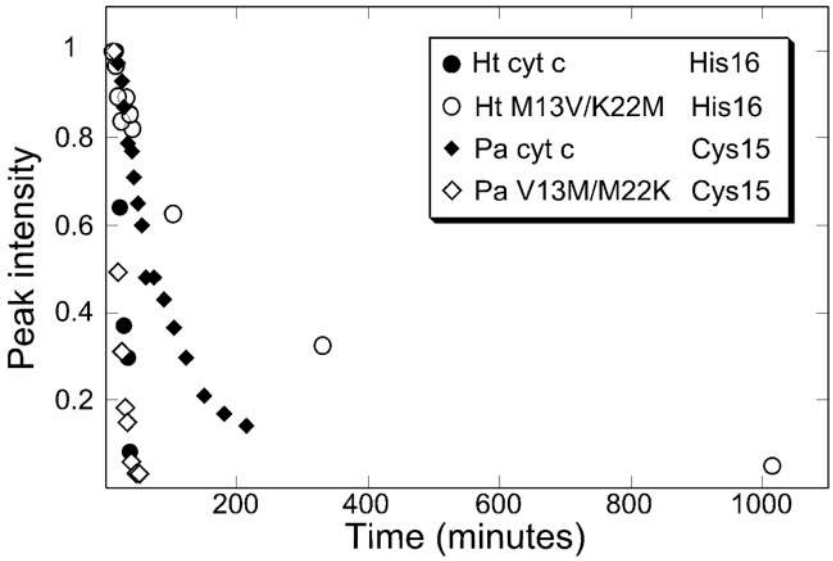

Figure 3.

Representative peak intensity data from HX experiments. Shown are plots of peak intensity (normalized) vs. time from HX initiation illustrating the difference in observed HX rate between His16 in *Ht*-M13V/K22M (open circles) relative to *Ht* cyt c_{552} (filled circles), and between Cys15 in *Pa*-V13M/M22K (open diamonds) relative to *Pa* cyt c_{551} (filled diamonds).

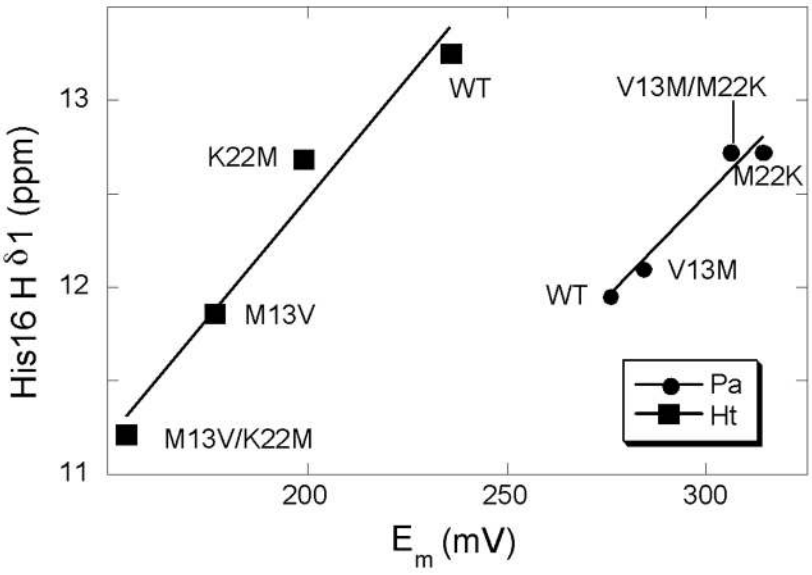

Figure 4.

Plot of His16 Hδ1 chemical shift vs. E_m for the wild-type (WT) proteins and six mutants. Data for *Pa* cyt c_{551} and mutants are plotted with circles, and data for *Ht* cyt c_{552} and mutants are plotted with squares. The lines demonstrate the linear fit, and have the same slope as each other (0.02 ppm/mV) within error.

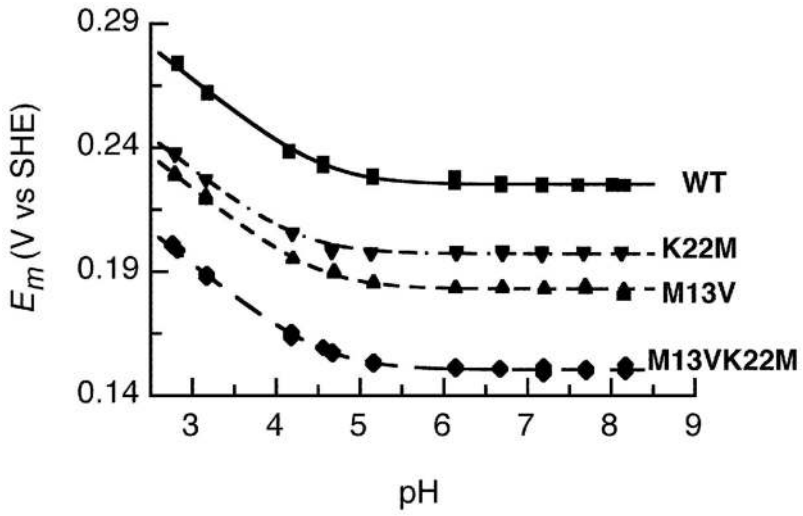

Figure 5.

E_m values of four *Ht* cyts c_{552}: WT (ν), M13V (σ), K22M (τ), and M13V/K22M(υ) as determined by PFV at 0°C, 50 mV/s, in phosphate containing buffer, as a function of pH. All data were acquired using a scan rate of 50 mV/s. pK_{red} values for wild type *Ht* cyt c_{552}, *Ht*-M13V, *Ht*-M22K, and *Ht*-M13V/K22M were found to be 4.2, 4.7, 4.2 and 4.3, respectively. Fitting was carried out as described previously (15).

Table 1

Log of protection factors (log *P*) for selected residues in wild-type and mutant proteins.

Residue	*Pa* cyt c_{551}				*Ht* cyt c_{552}			
	wild-type	**V13M**	**M22K**	**V13M/M22K**	**wild-type**	**M13V**	**K22M**	**M13V/K22M**
15	4.5	< 4.4[a]	5.1	3.4	< 3.4[b]	< 4.4[a]	< 4.4[a]	4.5
16	5.9	4.7	5.5	4.0	3.6	4.7	6.0	6.7
17	4.6	4.2	4.5	4.2	4.8	4.5	4.9	4.4

[a] exchanged before 8 hours (not detected in first TOCSY spectrum), upper limit given.

[b] exchanged before 13 minutes (not detected in first HSQC spectrum), upper limit given.

Table 2

Chemical shifts (ppm) of selected axial His nuclei at pH 7.0.

nucleus	*Pa* cyt c_{551}				*Ht* cyt c_{552}			
	wild-type	**V13M**	**M22K**	**V13M/M22K**	**wild-type**	**M13V**	**K22M**	**M13V/K22M**
Nδ1	169.3	171.1	171.6	173.2	182.3	170.5	181.3	167.1
Hδ1	11.9	12.1	12.7	12.7	13.2	11.8	12.7	11.2
Hε1	--[a]	--[a]	--[a]	--[a]	−16.4[b]	−17.6	−16.1	−17.5

[a] Not assigned

[b] Consistent with literature assignment (34).

Table 3

Electrochemical data for the wild-type and mutant proteins, comparing the midpoint potential at pH 7, and the interfacial electron transfer rate, k^0

Protein	Variant	E_m @ pH7 (mV)	k^0 (s^{-1})
Pa cyt c_{551}	wild-type	276 ± 2	1028 ± 117
	V13M	284 ± 2	1056 ± 142
	M22K	314 ± 2	921 ± 77
	V13M/M22K	306 ± 3	969 ± 119
Ht cyt c_{552}	wild-type	236 ± 2	1007 ± 128
	M13V	177 ± 1	1025 ± 112
	K22M	199 ± 1	1240 ± 74
	M13V/K22M	155 ± 2	1027 ± 124